Front. Mater. Sci. 2023, 17(4): 230665
https://doi.org/10.1007/s11706-023-0665-5

RESEARCH ARTICLE

Highly sensitive flexible strain sensor based on microstructured biphasic hydrogels for human motion monitoring

Xin Gao[1,2*], Xinyu Wang[2*], and Xingce Fan (✉)[1]

1 Key Laboratory of Quantum Materials and Devices of Ministry of Education, School of Physics, Southeast University, Nanjing 211189, China
2 School of Chemistry and Chemical Engineering, Southeast University, Nanjing 211189, China

ABSTRACT: Flexible strain sensors have been extensively used in human motion detection, medical aids, electronic skins, and other civilian or military fields. Conventional strain sensors made of metal or semiconductor materials suffer from insufficient stretchability and sensitivity, imposing severe constraints on their utilization in wearable devices. Herein, we design a flexible strain sensor based on biphasic hydrogel via an *in-situ* polymerization method, which possesses superior electrical response and mechanical performance. External stress could prompt the formation of conductive microchannels within the biphasic hydrogel, which originates from the interaction between the conductive water phase and the insulating oil phase. The device performance could be optimized by carefully regulating the volume ratio of the oil/water phase. Consequently, the flexible strain sensor with oil phase ratio of 80% demonstrates the best sensitivity with gauge factor of 33 upon a compressive strain range of 10%, remarkable electrical stability of 100 cycles, and rapid resistance response of 190 ms. Furthermore, the human motions could be monitored by this flexible strain sensor, thereby highlighting its potential for seamless integration into wearable devices.

KEYWORDS: flexible strain sensor; biphasic hydrogel; conductive hydrogel; human motion monitoring

Contents

Received July 31, 2023; accepted September 8, 2023

E-mail: fanxingce@126.com

* X.G. and X.W. contributed equally to this work.

1 Introduction

With the development of internet of things, flexible electronic devices have received extensive attention because of their potentials for portable, durable, and adaptable electronics across a wide range of applications [1–5]. Flexible strain sensors serve as an essential kind of

components in electronic devices, which have been designed to measure and detect mechanical strain or deformation in various scenarios, such as human motion detection [6–8], medical aids [9], electronic skins [10–11], and other civilian or military fields. Flexible strain sensors are generally fabricated by using materials that possess a certain level of stretchability while maintaining their performance integrity. Compared with conventional piezoelectric sensors [12–14] which suffer from inflexibility and brittleness, flexible strain sensors offer an alternative with advantages of adaptability, stretchability, and unrestricted bending, making them convenient to detect objects with complex morphologies.

The performances of flexible strain sensors are generally affected by many factors, among which the compositional materials and the device structures play crucial roles in the determination of the sensitivity, stretchability, response time, and other essential characteristics of flexible strain sensors. To date, several representative flexible strain sensors have been successfully developed, which employ conductive materials such as carbon nanotubes [15–17], metals/semiconductors [18–20], graphene [21–23], conductive polymers [24–26], and microfluidics [27] dispersed within soft and elastic matrices (such as polydimethylsiloxane (PDMS) [28–29], Ecoflex [21], and rubbers [30–31]), forming intricate permeable networks. However, high manufacturing cost, low fabrication efficiency, and complicated production process hinder the massive production and further applications of these flexible strain sensors.

In the recent decade, hydrogels owing to their remarkable flexibility, tunable mechanical properties, and exceptional biocompatibility have been extensively utilized in wearable electronic devices, such as electronic skin [32], soft robots [33], and flexible energy storage devices [34–35]. Researchers have successfully integrated diverse functional fillers including liquid metals [36–37], carbon nanotubes [38], and graphene [39] into the hydrogel matrix. They achieved changes in material conductivity by establishing connections between conductive and non-conductive phases of the fillers. Recently, Gao et al. [40] reported a high-performance flexible strain sensor by harnessing the microphase separation effect within biphasic hydrogels, comprising a conductive phase and an insulating phase to create highly extensible microstructure sensors. The application of external forces induces changes in the conductive microchannels present in the aqueous phase, leading to the attainment of ultrahigh electrical sensitivity. But there has been no exploration of a biphasic hydrogel system dominated by the insulating oil phase, where the conductive water phase is dispersed within it. Considering this unexplored avenue, it is possible that the utilization of such a system could pave the way for the development of a highly sensitive flexible strain sensor.

In this work, we design a new type of biphasic hydrogel flexible strain sensors, which is prepared through the *in-situ* polymerization of an oil/water emulsion system. The biphasic hydrogel is established by filling the insulating polymer matrix with conductive water, creating distinct conductive and insulating phases. The performance of the biphasic hydrogel can be simply modulated by altering the volume ratio of oil/water phase. By optimizing compositions of the biphasic hydrogel, the aqueous conductive microchannel in the biphasic hydrogel structure changes under external stress at the human body temperature, showing ultra-high electrical sensitivity and rapid response (gauge factor ~ 33). Additionally, the flexible strain sensor demonstrates rapid response characteristics, enabling real-time monitoring of human motions.

2 Results and discussion

Figure 1(a) shows the preparation process of biphasic hydrogel flexible strain sensors. A series of biphasic hydrogels with different stearyl methacrylate (SMA) volume fractions, 60, 70, 80, and 85 vol.%, were prepared and denoted as BH-Xs, where X represents the volume fraction of SMA. The BH-Xs were successfully synthesized through the *in-situ* radical polymerization of water-in-oil emulsion, incorporating hydrophilic monomers (acrylamide, AM, hydroxyethyl acrylate, HEA) along with lipophilic monomers SMA. The addition of an oil-soluble crosslinking agent (ethylene glycol dimethacrylate, EGDMA) and an emulsifier (sodium dodecylbenzenesulfonate, SDBS) facilitated the dissolution of the system at elevated temperatures, followed by the sonication for 5 min to achieve a stable water-in-oil emulsion. Subsequently, the polymerization was initiated by ammonium persulfate (APS) and resulted in the formation of a milky white opaque biphasic hydrogel (see Fig. S1). The components of BH-Xs and pure gel (G-100%) are shown in Table S1.

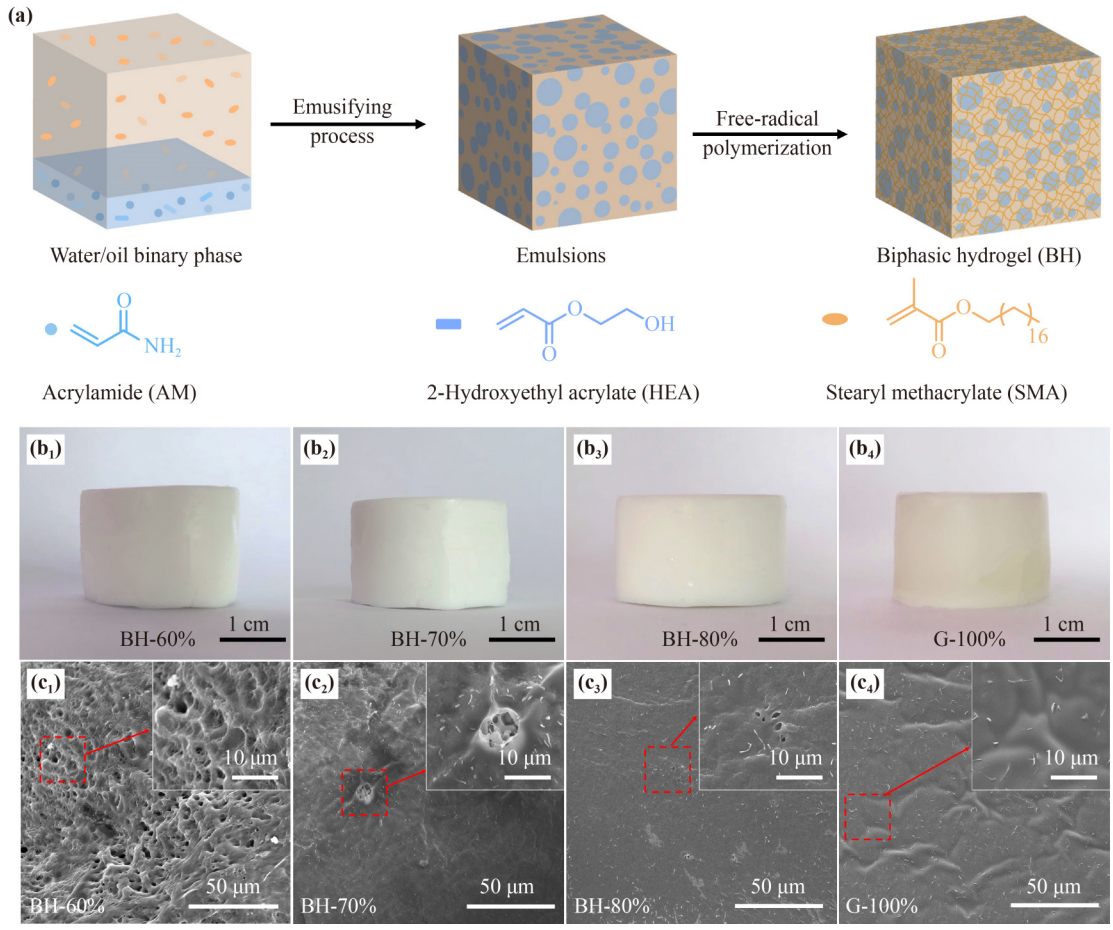

Fig. 1 Fabrication processes and characterizations of biphasic hydrogel flexible strain sensors. (**a**) Fabrication process of biphasic hydrogels by free-radical polymerization of emulsion. (**b**$_1$)(**b**$_2$)(**b**$_3$)(**b**$_4$) Photographs of biphasic hydrogel with different contents of SMA and the pure gel (G-100%). (**c**$_1$)(**c**$_2$)(**c**$_3$)(**c**$_4$) SEM images of BH-Xs and G-100% (the inset images are zoomed-in views of the red dashed box).

Figures 1(b$_1$)–1(b$_4$) depict the macroscopic morphology of BH-Xs (BH-60%, BH-70%, and BH-80%) and the control sample G-100%, all of which exhibit opaque milky white appearance. Scanning electron microscopy (SEM) images of BH-Xs and G-100% are shown in Figs. 1(c$_1$)–1(c$_4$). Following the emulsion gelation, the water takes different dispersion states within the SMA matrix based on the proportion of components. As a control, G-100% exhibits a uniform distribution of the SMA oil phase without the water dispersion. But for BH-60%, the distribution of water states with different sizes can be clearly observed, and the water primarily concentrates within the formed mesh structures. For BH-70%, the distribution range of water is reduced, yet the water state can still be observed. With an increase of the oil phase, BH-80% exhibits a further decrease in the water distribution. At this stage, the mesh structures disappear, and the water state is only dispersed within the discontinuous micropores. The varying ranges of water distribution states in biphasic hydrogels will yield significant disparities in their mechanical and sensing properties.

Excellent mechanical properties are essential for soft electronic skins, sensors, and devices [41–43]. To evaluate the mechanical properties of BH-Xs, we carried out strain–stress tests. As shown in Figs. 2(a$_1$)–2(a$_3$), the biphasic hydrogel displays high elasticity, enabling extensive compression and swift restoration to its original shape upon unloading. Figures 2(b) and S2 show the tensile properties of BH-Xs and G-100%, with BH-80% exhibiting the highest strain, surpassing 150%. Moreover, the modulus of BH-Xs gradually increases as the water phase content decreases (Table S2). Figure 2(d) highlights the compressive properties of BH-Xs and G-100%. Compared with G-100% which fractures at approximately 70% strain, the compressive mechanical properties of BH-Xs are effectively enhanced due to the existence of

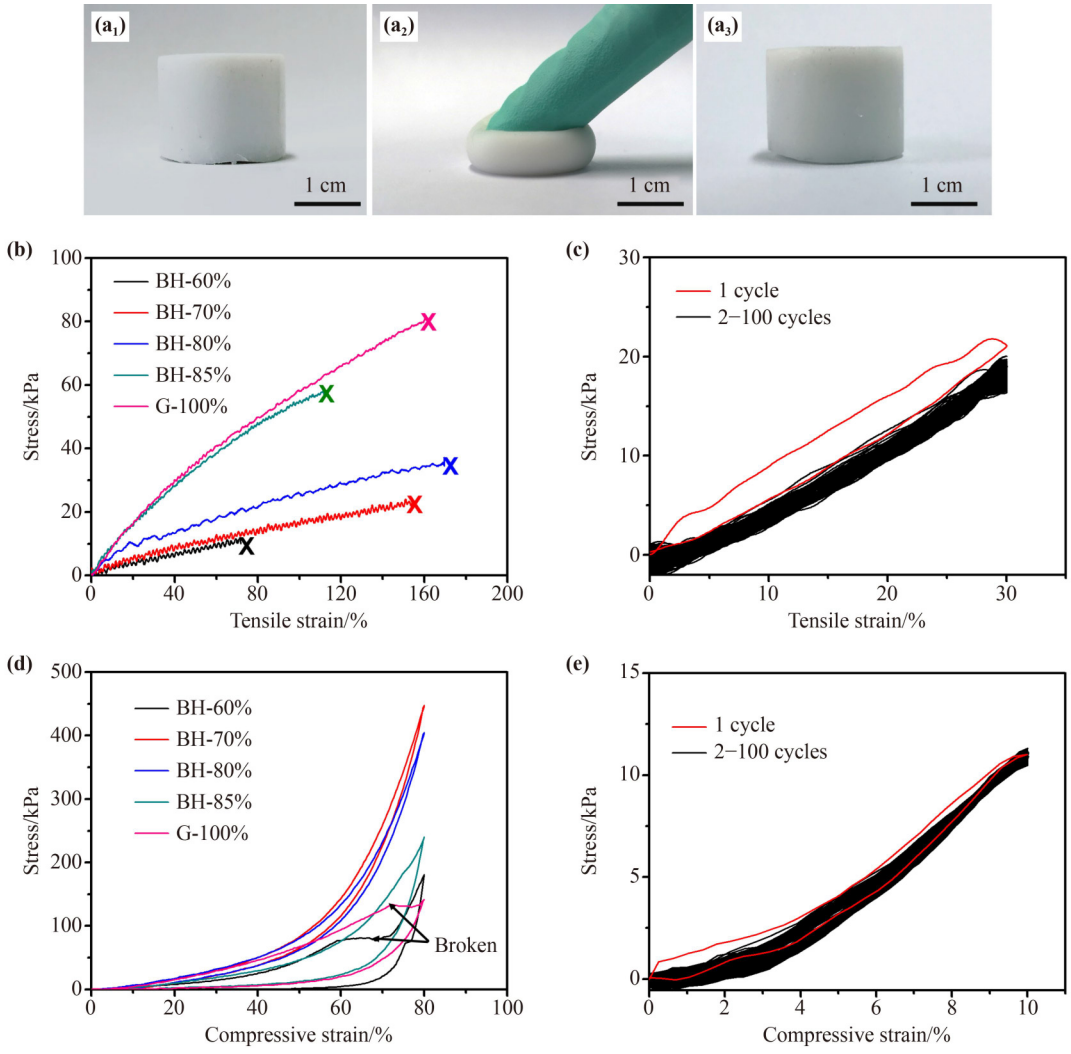

Fig. 2 Mechanical behaviors of BH-Xs and G-100% tested at 37 °C. (**a**$_1$)(**a**$_2$)(**a**$_3$) Images of the pressed BH-80%, showing its elasticity. (**b**) Tensile and (**d**) compressive stress–strain curves of BH-Xs and G-100%. (**c**) Tensile cyclic tests (100 cycles) for the BH-80% at a strain of 30%. (**e**) Compressive cyclic tests (100 cycles) for the BH-80% at a strain of 10%.

the biphasic structure. BH-70%, BH-80%, and BH-85% display the ability to withstand compression up to 80% strain, with the exception of BH-60%. The tensile and compressive curves of loading and unloading cycles are shown in Figs. 2(c) and 2(e). No significant change in their mechanical properties was observed after 100 loading and unloading cycles, indicating the excellent mechanical stability of the biphasic hydrogel.

Figure 3(a) shows strain–resistance curves of the compressive strain for BH-Xs (X = 60%, 70%, 80%, and 85%) at around the human body temperature (37 °C). Compression deformation results in reduced resistance across all biphasic hydrogels. BH-80% exhibits significantly higher sensitivity compared to BH-60%, BH-70%, and BH-85%. With an increase in the SMA content, the gauge factors (GF = $(\Delta R/R_0)/\sigma$) exhibit a trend of initial increase followed by decrease. Among them, BH-80% has the highest sensitivity of GF = 33, surpassing the sensitivity of many traditional sensors [41,44–45]. The difference in sensitivity among biphasic hydrogels with different SMA volume fractions is attributed to the structural difference of the conductive aqueous phase at the micropores formed upon the application of stress. Both BH-60% and BH-70% have relatively low sensitivities, with GF values of 3 and 14, respectively. As depicted in Figs. 3(b$_1$) and 3(b$_2$), BH-70% contains a relatively higher water content, forming a connected state, while it still remains in a conductive state under external stress, resulting in lower sensing sensitivity. In contrast, as shown in Figs. 3(c$_1$) and 3(c$_2$),

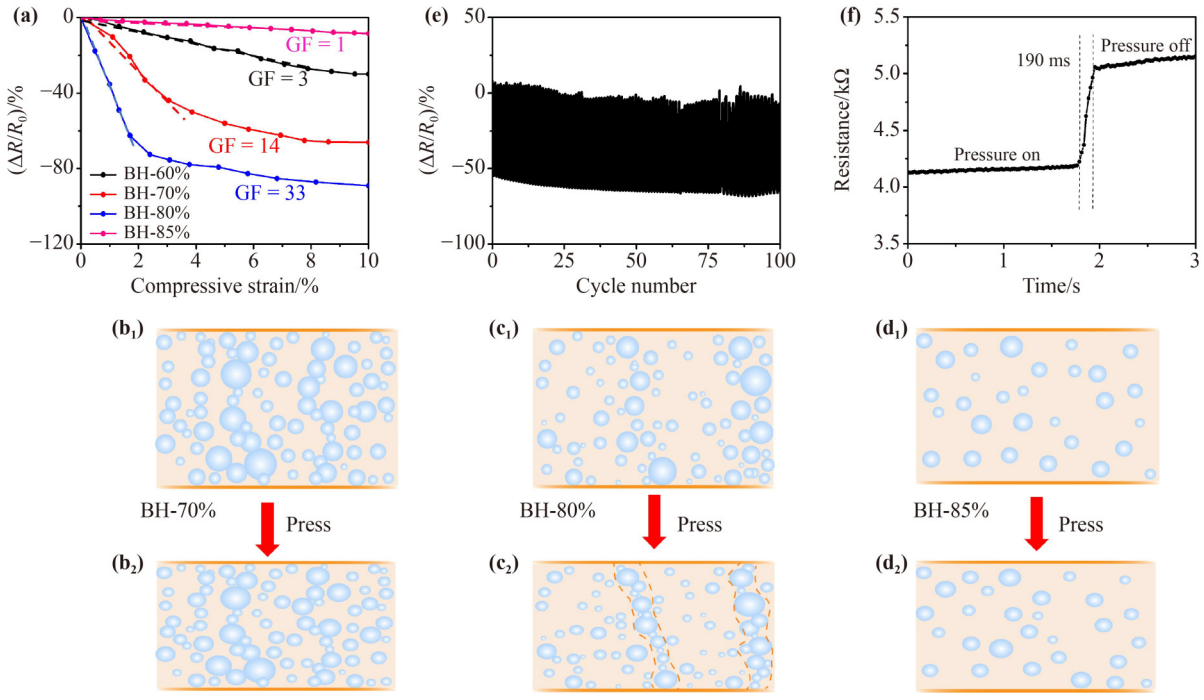

Fig. 3 Performances and working mechanisms of biphasic hydrogel flexible strain sensors. (**a**) Relative change in resistance of the BH-Xs strain sensor within compressive strain range of 0% to 10%. Schematic diagram for the deformation of the BH-Xs strain sensor with different contents of SMA: (**b$_1$**)(**b$_2$**) BH-70%; (**c$_1$**)(**c$_2$**) BH-80%; (**d$_1$**)(**d$_2$**) BH-85%. (**e**) Relative change in resistance under cyclic loading and unloading of 10% compressive strain for 100 cycles, showing the stability of the BH-80% flexible strain sensor. (**f**) Instant response of BH-80%, exhibiting response time of 190 ms.

BH-80% exhibits a reduced water content, resulting in the previously disconnected water regions to undergo structural changes under external stress. Consequently, these regions become interconnected, forming conductive pathways and resulting in higher sensing sensitivity. For BH-85%, the amount of water is insufficient, resulting in a disconnected state. Even when subjected to external stress, the water is still in a disconnected state, leading to a lower sensing sensitivity (Figs. 3(d$_1$) and 3(d$_2$)). However, when the water content was further reduced to a SMA volume fraction of 90 vol.%, the biphasic hydrogel could not be formed (Fig. S3).

Moreover, the biphasic hydrogel flexible strain sensor (BH-80%) demonstrates exceptional durability and fast response as shown in Figs. 3(e) and 3(f). Remarkably, it exhibits excellent electrical stability, as evidenced by the absence of significant resistance signal changes after subjecting it to 100 cycles of 10% compressive strain. Besides, it also exhibits an impressive response time of as fast as 190 ms under compressive stress. Moreover, the strain–resistance curves of tensile strain and durability for BH-Xs are shown in Figs. S4 and S5. Similarly, the biphasic hydrogel flexible strain sensor (BH-80%) exhibits significantly higher sensing sensitivity owing to the proper water content compared to those of BH-60%, BH-70%, and BH-85%.

The biphasic hydrogel flexible strain sensor, featuring excellent flexibility and high sensing sensitivity, is a promising candidate for comprehensive monitoring of human activities in wearable devices. As shown in Fig. 4, the biphasic hydrogel flexible strain sensor can detect large-ranged human body motions. The BH-80% strain sensor was attached to different joints of the human body, such as fingers, wrist, and elbow. The schematic diagrams presented in Figs. 4(a) and 4(b) depict the attachment of the BH-80% sensor to the outer and the inner sides of the finger, respectively. As the finger flexes and recovers, mimicking a stretching and compression cycle, a corresponding increase and decrease in the resistance signal are observed. Similarly, Figs. 4(c) and 4(d) show schematic diagrams of the BH-80% strain sensor attached to wrist and elbow joints, respectively. As the joints bend to a certain angle, different electrical signals are displayed, and the electrical signal returns to its initial value when the bending motion ceases.

In addition, the BH-80% strain sensor has the ability to detect and recognize minute human motions, including subtle muscle motions. This is exemplified in Fig. 5(a),

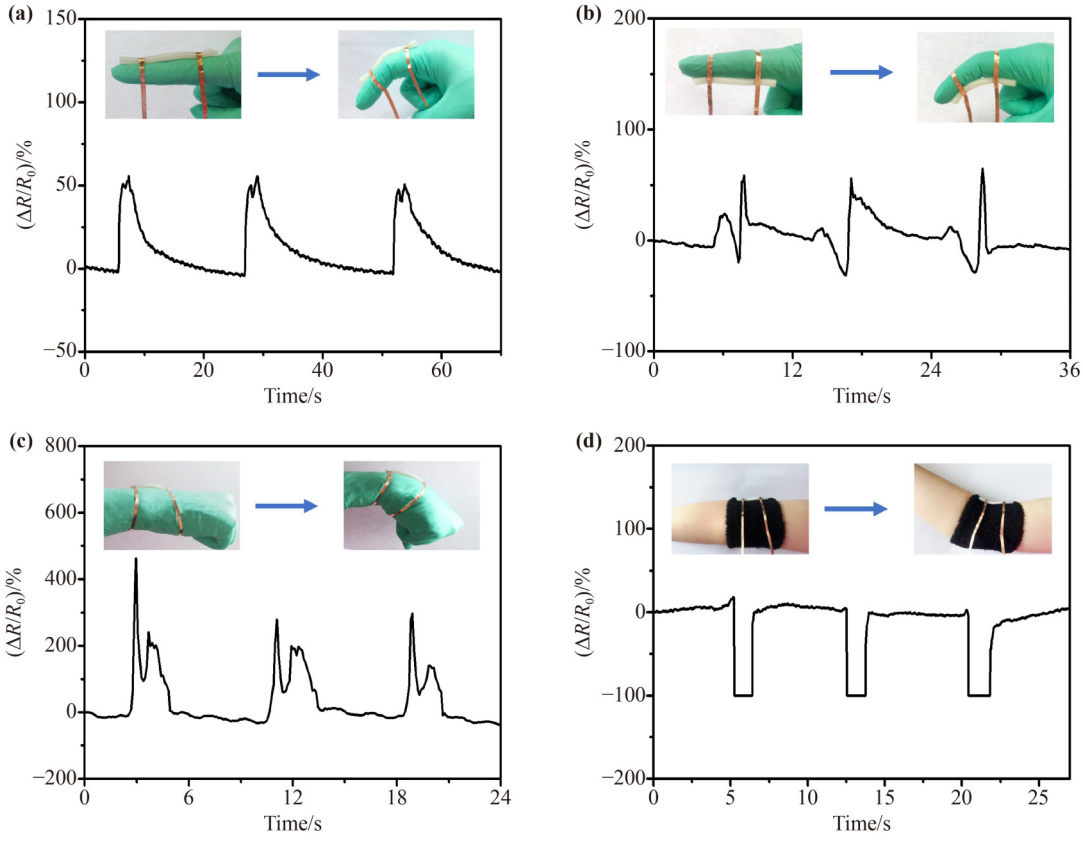

Fig. 4 Detection of various human motions using BH-80% flexible strain sensor. Relative change in resistance of the sensor assembled on (**a**) a bending finger outside, (**b**) finger inside, (**c**) wrist, and (**d**) elbow. The insets show the motions and sensing locations.

which reveals the performance of the BH-80% flexible strain sensor pasted at the mouth corner, enabling monitoring of facial expression changes. When transitioning from a neutral expression to a smile, discernible changes in the electrical signal were observed, which could be reliably reproduced. Figure 5(b) demonstrates the consistent and repetitive alterations in resistance as the researcher opened and closed his/her mouth. Additionally, by attaching the BH-80% flexible strain sensor at the corner of the mouth, as depicted in Figs. 5(c)–5(f), subtle muscle variations caused by pronouncing similar-sounding words (e.g., "chemical" *vs.* "chemistry") can bring about distinct electrical signal changes. Consequently, the biphasic hydrogel flexible strain sensor can accurately identify and generate different electrical signals.

Moreover, the water-in-oil biphasic hydrogel exhibits a shape memory behavior compared with the oil-in-water biphasic hydrogel reported by Gao et al. [40]. When placed in a high-temperature environment, the water-in-oil biphasic hydrogel exists in a soft elastic state, allowing it to be arbitrarily molded into various temporary shapes. As shown in Fig. S8, a long strip of biphasic hydrogel (BH-80%) was knotted at 70 °C. Then, it was rapidly cooled to fix shape at a lower temperature (25 °C) and still remained as the knotted configuration. Subsequently, the knotted biphasic hydrogel strip (BH-80%) was reheated to 70 °C and gradually restored the original long strip shape after 350 s owing to the interfacial tension between the oil/water phase and the intrinsic elasticity of the hydrogels.

3 Conclusions

In summary, we present an oil/water biphasic hydrogel flexible strain sensor prepared via *in-situ* polymerization of an emulsion system. The biphasic hydrogel is formed by incorporating a conductive water phase into an insulating oil phase. Different volume ratios of the oil and water phases give rise to distinct phase structures within the biphasic hydrogels. The biphasic hydrogel flexible

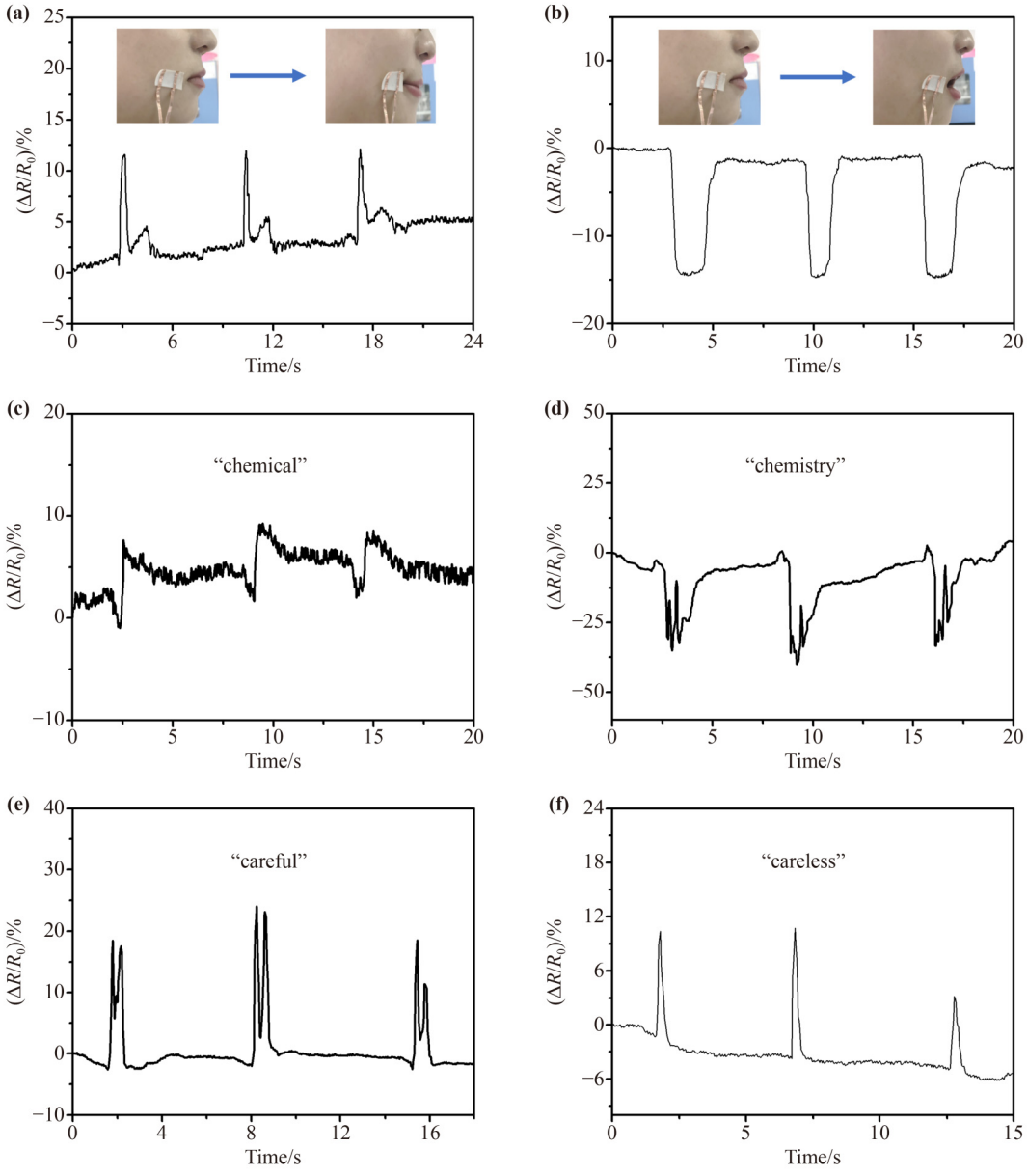

Fig. 5 Detection of various subtle human motions with BH-80% flexible strain sensor. (**a**) Relative resistance changes when the researcher smiled. (**b**) Relative resistance changes during opening and closing the mouth. (**c**)(**d**)(**e**)(**f**) Relative resistance changes when the researcher spoke different words. The insets show the motions and sensing locations.

strain sensor shows remarkable properties when compared to conventional strain sensors. Within a compressive strain range of 10%, the biphasic hydrogel sensor with the oil phase ratio of 80% exhibits a substantial gauge factor of 33. Remarkable electrical stability of 100 cycles and rapid resistance response of 190 ms were also achieved. Furthermore, the biphasic hydrogel flexible strain sensor exhibits excellent signal responsiveness, stability and repeatability when utilized for detecting human motions, including joint motions, such as those in fingers, facial expressions and the speaking. This biphasic hydrogel flexible strain sensor can be potentially used in wearable devices, soft robots, motion monitoring, medical treatment and other related fields. In addition, the concept of biphasic hydrogels is also demonstrated effective in high-performance photocatalysis owing to their macroporous matrix configurations, which can increase the loading amount of photocatalysts and improve the mass transfer efficiency [46–47]. Furthermore, the hydrogel matrix has the flexibility to accomodate various types of filler materials, which also give the chance to develop highly efficient photocatalysts.

Experimental section

Materials 2, 2′-Azobis (2-methylpropionitrile) (AIBN) (98%), acrylamide (AM) (AR, 99%), sodium dodecylbenzenesulfonate (SDBS) (95%, mixture), and 2-hydroxyethyl acrylate (HEA) (96%) were purchased from Aladdin Co., Ltd. Ammonium persulfate (APS) (AR, 98%) were supplied by Sinopharm Group Chemical Reagent Co., Ltd. Stearyl methacrylate (SMA) (AR, 95%) were purchased from Energy Chemical. Ethyleneglycol dimethacrylate (EGDMA) was supplied by Shanghai D&B Biological Science and Technology Co., Ltd.

Preparation of the control Gel (G-100%) 3.456 g SMA, 0.050 g SDBS, 0.009 g EGDMA, and 0.030 g AIBN were mixed in a 10 mL vial. Then, the mixture was stirred at 50 °C to form a uniform solution. The solution was initiated in a 70 °C oven for 3 h to obtain the cylinder-shaped gel.

Preparation of biphasic hydrogels (BH-Xs) Taking BH-60% as an example, in a 10 mL vial, 0.200 g AM, 3.456 g SMA, 0.05 g SDBS, 0.009 g EGDMA, and 0.088 g HEA were distributed in 2.67 mL distilled water. Then, the mixture was stirred at 50 °C to form a uniform solution. After that, the solution was homogenized by the ultrasonic crushing for 5 min to form the opalescent precursor (see Fig. S1 for more details). Finally, 20 mg APS was added into the precursor and initiated the gelation in a 70 °C oven for 3 h to obtain cylinder-shaped BH-60%. In this work, cylinder-shaped biphasic hydrogels loaded with 60, 70, 80, and 85 vol.% SMA were prepared via the similar fashion but with different volume ratios of SMA and distilled water.

Mechanical property measurements The tensile and compressive tests were all conducted on a SANS E42.503 tensile tester at the speed of 30 mm·min^{-1}. The tensile and compressive samples are long bars (Φ = (4.0±0.2) mm, L = (50.9±3.1) mm) and cylinders (Φ = (17.65±0.5) mm, L = (13.2±0.6) mm), respectively. The fixtures on MTS E42 were removable and fixture-choosing depended on the test type, tension or compression. All reported values for mechanical properties represented an average over at least three independent measurements for each sample.

Ultrasonic crashing In all reported ultrasonic processes of this work, a Biosafer 150-96 ultrasonic crasher was utilized, power at 45%. Samples were all sonicated for 5 min.

Scanning electron microscopy (SEM) application Specimens for SEM studies were first placed in liquid nitrogen by tweezers, and then instantly transferred into a freeze-dryer (LC-10N-50A with a 2XZ-2 rotary vane vacuum pump) for 18 h to remove all water in the hydrogels. The cross-sectional images of the resulted specimens were taken consequently.

Resistance measurements The plot of resistance–time curve was monitored by the Keysight 34461A on a two-wire mode. The number of power line cycles (NPLC) and measurement range is 0.02 and automatic mode while the measurement option is Resistance 2 W. The heating jacket (Fig. S6) and the heating stage (Fig. S7) were used to control the environment temperature (around the body temperature, 37 °C). When the compressive and tensile tests were carried out, both sides of BH were linked by flexible copper electrodes. Meanwhile, the other sides of both copper electrodes were connected to the Keysight 34461A. As shown in Fig. S7, the cylinder-shaped BH (Φ = 17.65 mm, h = 13.25 mm) was used for the compressive test, and the device contained a sandwich structure (from top to bottom: fixture seats, PTFE film, and copper foil). The PTFE film was acted as an insulator. In the tensile test, while attached by copper electrodes and rubber (as a buffer and insulator), two of four fixtures were on the upper and lower ends, respectively. The configuration also had a sandwich structure with flexible copper (electrode), rubber (buffer and insulator), and fixture (a part of MTS E42) in turns from inside to outside. The specimen was adhered on copper electrodes by screwing fixtures. As shown in the insets of Fig. 4, BH-80% (Φ = 4.03 mm, L = 50.85 mm) was placed on the human joint to sense the human joint bending action, and the responses were monitored by instrument when the joint was bent or stretched. In the same strategy, as shown in the insets of Fig. 5, the rectangle specimen (25.0 mm × 14.3 mm × 1.1 mm) was used for resistance sensing derived from facial muscle motions. In the processes mentioned above, all the wires were fixed firmly by insulating tapes.

Authors' contributions Xin Gao — conceptualization, investigation, methodology, and writing-original draft; Xinyu Wang — conceptualization, investigation, methodology, and writing-original draft; Xingce Fan — writing-original draft, writing-review & editing, funding acquisition, and supervision.

Declaration of competing interests The authors declare that they have no competing interests.

Acknowledgements Xingce Fan acknowledges the China Postdoctoral Science Foundation (Grant No. 2021M700773) and the Jiangsu Planned

Projects for Postdoctoral Research Funds (Grant No. 2021K509C). The authors thank Prof. Jiuyang Zhang for the help of experimental tests and fruitful discussions.

Electronic supplementary information Supplementary materials can be found in the online version at https://doi.org/10.1007/s11706-023-0665-5 and https://journal.hep.com.cn/foms/EN/10.1007/s11706-023-0665-5, which include Figs. S1–S8 and Tables S1–S2. Following information is provided: optical images of biphasic hydrogels with SMA percentages of 80% and 90% via emulsion polymerization process; table of components of BH-Xs and G-100%; optical image of pristine and stretched biphasic hydrogels of BH-80%; table of tensile properties of BH-Xs and G-100%; tensile strain–resistance curves of BH-60%, BH-70%, BH-80%, and BH-85%; tensile electrical cyclic curves of BH-80% for 100 times; optical image of tensile test and its setup; optical image of the compressive test and its setup.

References

[1] Zheng B H, Zhou H W, Wang Z, et al. Fishing net-inspired mutiscale ionic organohydrogels with outstanding mechanical robustness for flexible electronic devices. Advanced Functional Materials, 2023, 33(28): 2213501

[2] Xiao X, Zheng Z Y, Zhong X W, et al. Rational design of flexible Zn-based batteries for wearable electronic devices. ACS Nano, 2023, 17(3): 1764–1802

[3] Gong X F, Chu Z Y, Li G C, et al. Efficient fabrication of carbon nanotube-based stretchable electrodes for flexible electronic devices. Macromolecular Rapid Communications, 2023, 44(5): 2200795

[4] Wu Y, Chen C, Meng Y, et al. Flexible carbon-based 3D conductive network structure blade-coated on poly(ethylene terephthalate) substrate for light-emitting electronic devices. Advanced Engineering Materials, 2022, 24(7): 2101355

[5] Lu J, Gu J F, Hu O D, et al. Highly tough, freezing-tolerant, healable and thermoplastic starch/poly(vinyl alcohol) organohydrogels for flexible electronic devices. Journal of Materials Chemistry A: Materials for Energy and Sustainability, 2021, 9(34): 18406–18420

[6] Li H, Cao J Q, Chen J L, et al. Highly sensitive MXene helical yarn/fabric tactile sensors enabling full scale movement detection of human motions. Advanced Electronic Materials, 2022, 8(4): 2100890

[7] Lu X Y, Qin Y F, Chen X Z, et al. An ultra-wide sensing range film strain sensor based on a branch-shaped PAN-based carbon nanofiber and carbon black synergistic conductive network for human motion detection and human-machine interfaces. Journal of Materials Chemistry C: Materials for Optical and Electronic Devices, 2022, 10(16): 6296–6305

[8] Zong Y, Tan S, Ma J Z. Flame-retardant PEDOT:PSS/LDHs/leather flexible strain sensor for human motion detection. Macromolecular Rapid Communications, 2022, 43(8): 2100873

[9] Pendley B D, Lindner E. Designing medical, point of care sensors to aid health care providers in diagnosing and managing diseases: addressing pertinent issues and some contemporary opportunities. Electroanalysis, 2018, 30(2): 310–313

[10] Zhao X L, Hua Q L, Yu R M, et al. Flexible, stretchable and wearable multifunctional sensor array as artificial electronic skin for static and dynamic strain mapping. Advanced Electronic Materials, 2015, 1(7): 1500142

[11] Peng W W, Han L, Huang H L, et al. A direction-aware and ultrafast self-healing dual network hydrogel for a flexible electronic skin strain sensor. Journal of Materials Chemistry A: Materials for Energy and Sustainability, 2020, 8(48): 26109–26118

[12] Han C, Zhang H, Chen Q, et al. A directional piezoelectric sensor based on anisotropic PVDF/MXene hybrid foam enabled by unidirectional freezing. Chemical Engineering Journal, 2022, 450(11): 138280

[13] Wu J T, Ye F, Hugo F, et al. Strain response of a semi-rigid base asphalt pavement based on heavy-load full-scale accelerated pavement testing with fibre Bragg grating sensors. Road Materials and Pavement Design, 2015, 16(2): 316–333

[14] Jin T Y, Park S H K, Fang D W, et al. Highly-stable flexible pressure sensor using piezoelectric polymer film on metal oxide TFT. RSC Advances, 2022, 12(33): 21014–21021

[15] Lee J, Lim M, Yoon J, et al. Transparent, flexible strain sensor based on a solution-processed carbon nanotube network. ACS Applied Materials & Interfaces, 2017, 9(31): 26279–26285

[16] Song Y, Lee J I, Pyo S, et al. A highly sensitive flexible strain sensor based on the contact resistance change of carbon nanotube bundles. Nanotechnology, 2016, 27(20): 205502

[17] Kanoun O, Muller C, Benchirouf A, et al. Flexible carbon nanotube films for high performance strain sensors. Sensors, 2014, 14(6): 10042–10071

[18] Chen J, Zhang J J, Luo Z B, et al. Superelastic, sensitive, and low hysteresis flexible strain sensor based on wave-patterned liquid metal for human activity monitoring. ACS Applied Materials & Interfaces, 2020, 12(19): 22200–22211

[19] Wu H P, Qi H C, Wang X, et al. Stretchable, sensitive, flexible strain sensor incorporated with patterned liquid metal on hydrogel for human motion monitoring and human–machine interaction. Journal of Materials Chemistry C: Materials for Optical and Electronic Devices, 2022, 10(21): 8206–8217

[20] Ji T, Jung S, Varadan A K. Field-controllable flexible strain sensors using pentacene semiconductors. IEEE Electron Device Letters, 2007, 28(12): 1105–1107

[21] Kim S J, Mondal S, Min B K, et al. Highly sensitive and flexible strain–pressure sensors with cracked paddy–shaped MoS_2/

graphene foam/Ecoflex hybrid nanostructures. ACS Applied Materials & Interfaces, 2018, 10(42): 36377–36384

[22] Wang Y M, Wang Y, Yang Y. Graphene–polymer nanocomposite-based redox-induced electricity for flexible self-powered strain sensors. Advanced Energy Materials, 2018, 8(22): 1800961

[23] Chen B L, Liu Y, Wang G S, et al. Low-cost flexible strain sensor based on thick CVD graphene. Nano, 2018, 13(11): 1850126

[24] Chen X Y, Zhang X Z, Xiang D, et al. 3D printed high-performance spider web-like flexible strain sensors with directional strain recognition based on conductive polymer composites. Materials Letters, 2022, 306(11): 130935

[25] Pan Z Y, Ma J Z, Zhang W B, et al. Flexible conductive polymer composites in strain sensors. Progress in Chemistry, 2020, 32(10): 1592–1607

[26] Cochrane C, Lewandowski M, Koncar V. A flexible strain sensor based on a conductive polymer composite for *in situ* measurement of parachute canopy deformation. Sensors, 2010, 10(9): 8291–8303

[27] Yeo J C, Yu J H, Koh Z M, et al. Wearable tactile sensor based on flexible microfluidics. Lab on a Chip, 2016, 16(17): 3244–3250

[28] Zhang C J, Li H, Huang A M, et al. Rational design of a flexible CNTs@PDMS film patterned by bio-inspired templates as a strain sensor and supercapacitor. Small, 2019, 15(18): 1805493

[29] Gong X X, Fei G T, Fu W B, et al. Flexible strain sensor with high performance based on PANI/PDMS films. Organic Electronics, 2017, 47(11): 51–56

[30] Qu M C, Qin Y J, Sun Y, et al. Biocompatible, flexible strain sensor fabricated with polydopamine-coated nanocomposites of nitrile rubber and carbon black. ACS Applied Materials & Interfaces, 2020, 12(37): 42140–42152

[31] Tadakaluru S, Thongsuwan W, Singjai P. Stretchable and flexible high-strain sensors made using carbon nanotubes and graphite films on natural rubber. Sensors, 2014, 14(1): 868–876

[32] Wang M C, Zhou H W, Jin X L, et al. Highly compliant and low strain hysteresis sensory electronic skins based on solution processable hybrid hydrogels. Journal of Materials Chemistry C: Materials for Optical and Electronic Devices, 2021, 9(5): 1822–1828

[33] Cheng Y, Chan K H, Wang X Q, et al. Direct-ink-write 3D printing of hydrogels into biomimetic soft robots. ACS Nano, 2019, 13(11): 13176–13184

[34] Ma Y, Yang C X, Liang E X, et al. Facile synthesis of ultra-tensile hydrogels for flexible all-solid-state supercapacitor energy storage devices. Journal of Sol-Gel Science and Technology, 2022, 103(2): 335–344

[35] Zheng L X, Guan L T, Yang G, et al. One-pot synthesis of $CoFe_2O_4$/rGO hybrid hydrogels with 3D networks for high capacity electrochemical energy storage devices. RSC Advances, 2018, 8(16): 8607–8614

[36] Zhang Z X, Tang L, Chen C, et al. Liquid metal-created macroporous composite hydrogels with self-healing ability and multiple sensations as artificial flexible sensors. Journal of Materials Chemistry A: Materials for Energy and Sustainability, 2021, 9(2): 875–883

[37] Fan L L, Duan M H, Xie Z C, et al. Injectable and radiopaque liquid metal/calcium alginate hydrogels for endovascular embolization and tumor embolotherapy. Small, 2020, 16(2): 1903421

[38] Qin Z H, Sun X, Yu Q Y, et al. Carbon nanotubes/ hydrophobically associated hydrogels as ultrastretchable, highly sensitive, stable strain, and pressure sensors. ACS Applied Materials & Interfaces, 2020, 12(4): 4944–4953

[39] Zhang Z, Lucia L. Toward synergistic reinforced graphene nanoplatelets composite hydrogels with self-healing and multi-stimuli responses. Polymer, 2021, 234(11): 124228

[40] Gao T L, Gao X, Li T Q, et al. Microstructured biphasic hydrogels for highly sensitive and asymmetric sensors with temperature-dependent sensitivity. Journal of Polymer Science, 2022, 60(18): 2701–2709

[41] Amjadi M, Kyung K U, Park I, et al. Stretchable, skin-mountable, and wearable strain sensors and their potential applications: a review. Advanced Functional Materials, 2016, 26(11): 1678–1698

[42] Wang T, Zhang Y, Liu Q, et al. A self-healable, highly stretchable, and solution processable conductive polymer composite for ultrasensitive strain and pressure sensing. Advanced Functional Materials, 2018, 28(7): 1705551

[43] Duan J, Liang X, Guo J, et al. Ultra-stretchable and force-sensitive hydrogels reinforced with chitosan microspheres embedded in polymer networks. Advanced Materials, 2016, 28(36): 8037–8044

[44] Wang Y, Yang R, Shi Z, et al. Super-elastic graphene ripples for flexible strain sensors. ACS Nano, 2011, 5(5): 3645–3650

[45] Zhang Y Z, Lee K H, Anjum D H, et al. MXenes stretch hydrogel sensor performance to new limits. Science Advances, 2018, 4(6): eaat0098

[46] Lee W H, Lee C W, Cha G D, et al. Floatable photocatalytic hydrogel nanocomposites for large-scale solar hydrogen production. Nature Nanotechnology, 2023, 18(7): 754–762

[47] Li X, Liu J, Jiang G C, et al. Self-supported $CsPbBr_3/Ti_3C_2T_x$ MXene aerogels towards efficient photocatalytic CO_2 reduction. Journal of Colloid and Interface Science, 2023, 643(11): 174–182